

# Knitted self-powered sensing textiles for machine learning-assisted sitting posture monitoring and correction

Yang Jiang<sup>1,2,§</sup>, Jie An<sup>1,2,§</sup>, Fei Liang<sup>3,§</sup>, Guoyu Zuo<sup>4</sup>, Jia Yi<sup>1,2</sup>, Chuan Ning<sup>1,2</sup>, Hong Zhang<sup>4</sup>, Kai Dong<sup>1,2</sup> (✉), and Zhong Lin Wang<sup>1,2,5</sup> (✉)

<sup>1</sup> Beijing Institute of Nanoenergy and Nanosystems, Chinese Academy of Sciences, Beijing 101400, China

<sup>2</sup> School of Nanoscience and Technology, University of Chinese Academy of Sciences, Beijing 100049, China

<sup>3</sup> Institute of Textiles and Clothing, The Hong Kong Polytechnic University Hung Hom, Kowloon, Hong Kong 999077, China

<sup>4</sup> Faculty of Information Technology, Beijing University of Technology, Beijing 100124, China

<sup>5</sup> School of Materials Science and Engineering, Georgia Institute of Technology, Atlanta, GA 30332-0245, USA

<sup>§</sup> Yang Jiang, Jie An, and Fei Liang contributed equally to this work.

© Tsinghua University Press 2022

Received: 16 February 2022 / Revised: 6 April 2022 / Accepted: 7 April 2022

## ABSTRACT

With increasing work pressure in modern society, prolonged sedentary positions with poor sitting postures can cause physical and psychological problems, including obesity, muscular disorders, and myopia. In this paper, we present a self-powered sitting position monitoring vest (SPMV) based on triboelectric nanogenerators (TEGs) to achieve accurate real-time posture recognition through an integrated machine learning algorithm. The SPMV achieves high sensitivity (0.16 mV/Pa), favorable stretchability (10%), good stability (12,000 cycles), and machine washability (10 h) by employing knitted double threads interlaced with conductive fiber and nylon yarn. Utilizing a knitted structure and sensor arrays that are stitched into different parts of the clothing, the SPMV offers a non-invasive method of recognizing different sitting postures, providing feedback, and warning users while enhancing long-term wearing comfortability. It achieves a posture recognition accuracy of 96.6% using the random forest classifier, which is higher than the logistic regression (95.5%) and decision tree (94.3%) classifiers. The TENG-based SPMV offers a reliable solution in the healthcare system for non-invasive and long-term monitoring, promoting the development of triboelectric-based wearable electronics.

## KEYWORDS

posture monitoring, knitted fabric, triboelectric nanogenerator, wearable electronics, machine learning

## 1 Introduction

Recently, substantial stress and pressure during work or education have caused individuals to adopt a sedentary lifestyle. Sitting in a poor posture for extended periods can cause physical and psychological problems, such as spine disease, obesity, muscular disorders, and myopia [1–4]. Therefore, common techniques, such as vision-based methods using cameras, are applied to identify the sitting postures of individuals to decrease the risk of back pain, especially for students and office workers [5, 6]. However, the vision-based recognition method has specific illumination requirements and is unable to continuously record the postures if the individual goes outside the frame of cameras. For example, Michael Wolfram developed a visual focus recognition camera that could be placed on the heads of users [7]. However, considering that this technique does not control the illumination of the room, the image quality is affected, which in turn decreases the accuracy. Therefore, a portable and convenient sensor with an intervention function that reminds users to maintain the right posture is required to track sitting posture during a sustained working period.

Owing to the miniaturization and integration of electronics and

wireless sensing networks, wearable electronics are gradually utilized in health monitoring and human posture recognition to address the aforementioned drawbacks [8–14]. In particular, textile-based wearable sensors have recently received special attention, since they can be woven into clothes for real-time monitoring of motion and physiological signals [15–17]. Conventional tactile wearable sensors are based on piezoresistive, piezoelectric, and capacitive devices [18–24]. However, these sensors have a complex fabrication process and an unpleasant wearing experience due to the utilization of rigid materials in the sophisticated micro-electro-mechanical system process technology. To ensure stability, most of these sensors utilize rigid substrates, such as printed circuit boards, that are uncomfortable for users [25–27]. Although some attempts replacing rigid electronic components with soft substrates to improve flexibility, the connection between the soft and rigid materials produces hotspots and non-linearity under stretching and bending [28–31]. In addition, these sensors are driven by external power sources that increase energy consumption. To mitigate the aforementioned shortcomings, researchers seek new materials and techniques that offer additional compatibility and wearable sensors with harmonious human–computer interaction for constant health interventions.

Fortunately, a new electromechanical conversion technology invented by Wang's group in 2012, known as triboelectric nanogenerator (TENG) [32–35], has been considered as self-powered sensors. The TENG exhibits high electric output in low frequency, good sensitivity, and microscale motion detection that can catch weak physiological signals from the human body [36–40]. Moreover, twisting or bending TENGs may cause contact–separation between different materials, which can be converted into electric signals based on the coupling effect of triboelectrification and electrostatic induction. Therefore, by integrating TENGs into clothing, the resultant device can recognize human action by generating corresponding electrical signals.

For better identification of the sitting posture, a correlation model should be built between the human posture and electrical signals. Rapid advancements in machine learning present multiple opportunities to solve this problem [6, 41–45]. Based on iterative learning and training using large samples, an exact mathematical mapping function can be built even with vague physical signal dates, allowing the well-trained model to effectively identify movement and conduct accurate posture prediction.

In this study, we develop a self-powered sitting position monitoring vest (SPMV) by collecting energy from individual motions. The proposed SPMV is manufactured using double weft-knitted fabric (nylon yarns and conductive fibers), which can generate electrical signals through contact–separation between fibers by triboelectrification and electrostatic induction. Due to the knitted structure design, the SPMV achieves good stretchability, softness, and comfort. To improve posture recognition accuracy, sensors are stitched into various parts of the clothing to record deformation in different parts of the human body and present real-time signal processing and posture recognition feedback to its users. Using the random forest classifier, the proposed SPMV achieves a posture recognition accuracy of 96.6% (higher than both logistic regression (95.5%) and decision tree (94.3%) classifiers). Therefore, the proposed TENG-based wearable textile sensing SPMV offers a reliable solution for adjusting sitting posture, promoting the application of triboelectric-based wearable electronics.

## 2 Experimental sections

### 2.1 Fabrication of SPMV

The conductive fibers were made of Ag wires that surface was coated by polytetrafluoroethylene. The nylon yarn and the conductive fibers were woven into one-to-one cross double-threaded knitting loops. Thereafter, the sensors were sewed into a sporty vest that exhibited high stretchability. Finally, a layer of cotton in the shape of a five-pointed star was placed over the top to cover and protect the sensors.

### 2.2 Characterization and measurement

A step motor (LinMot E1100) was applied to provide the periodic contact–separation movement for TENGs. A programmable electrometer (Keithley, model 6514) was adopted to test the voltage, current, and charge. The software platform was constructed on LabView and Python as they were capable of realizing real-time data acquisition.

The corresponding signal data were collected and processed by the machine learning algorithm. First, the data sets were processed using fast Fourier transform and formed multiple training sets. Thereafter, these sets were trained using random decision tree to form a random forest that classified the sitting position through the voting decisions of multiple decision trees. Finally, the real-

time changes in the sitting posture of the user were presented in the screen.

## 3 Results and discussion

### 3.1 Fabrication and structure of the SPMV

Although a prolonged sedentary lifestyle is prevalent worldwide, consistently sitting with incorrect or unhealthy states is more likely to cause spinal deformity and asymmetry, which increases the risk of multiple illnesses, such as musculoskeletal, cardiovascular, and cerebrovascular diseases (strokes). People often sit in various poor postures in their daily life, such as humpback, hypokinesia, and upper body leaning toward the right or left, thereby experiencing musculoskeletal pain, which can arise from the classroom environment. This “sitting disease” could be alleviated if individuals could observe their real-time sitting posture by wearing a specific type of clothing. Figure 1(a) illustrates the process for real-time monitoring of the sitting posture using the SPMV. When the user sits in front of the desk wearing the SPMV, they can watch their sitting posture change on their screen. In a sitting position, different parts of the human body undergo different movements and deformations. Therefore, to improve posture recognition accuracy, multiple SPMVs are positioned on different parts of the cervical spine, thoracic spine, and lumbar spine. Figure 1(b) displays the interlock stitch knitted loops between the nylon yarn and the conductive fiber of the SPMV. Figure 1(c) demonstrates normal function of the SPMV despite being stretched, twisted, rolled, and bended. Figure 1(d) shows a photograph of the user wearing the SPMV (eight sensors).

### 3.2 Working principle of the SPMV

Figure 2(a) demonstrates the working process of a textile sensor under finger pressing. Based on the conjunction of triboelectrification and electrostatic induction, Fig. 2(b) shows the working mechanism of the SPMV. The SPMV works in a single-electrode mode wherein its conductive fibers are connected to the ground by a conductive wire. Due to the stretchable knitted loop structure, the SPMV can work under two conditions: compression and stretchability. In the event of applied external force or the user stretching the SPMV, the two fibers undergo deformation and establish contact with each other. The analysis of the electricity-generating process is clearer in the cross-sectional area. When the conductive fiber and the nylon yarn establish contact, an electrification process occurs at their interface (Fig. 2(b)(I)), thereby generating equivalent charges with opposite polarities on the contact surface of the two fibers. The conductive fiber gains a negative triboelectric charge since it has a higher ability to capture negative charges, whereas the nylon yarn gains a positive charge. Upon separating the two yarns, the electrostatic induction effect induces a positive charge in the inner conductive fibers (Fig. 2(b)(II)). As the separation begins, the potential difference increases, resulting in an instantaneous electron flow from the conductive yarns to the ground. The electron flow continues until the two fibers separate completely (Fig. 2(b)(III)). Figure 2(b)(IV) demonstrates that when the nylon yarn establishes contact with the conductive fiber again, the electrons flow back from the ground to the conductive fiber. This continuous contact and separation movement between the two fibers generates an alternating current. To acquire the electricity-generating process, we conduct corresponding simulations of potential distributions for every component in the contact and separation states using the COMSOL software. Figure 2(c) demonstrates a small potential that is generated when the two yarns establish contact. As the two yarns separate and the corresponding potential increases, the

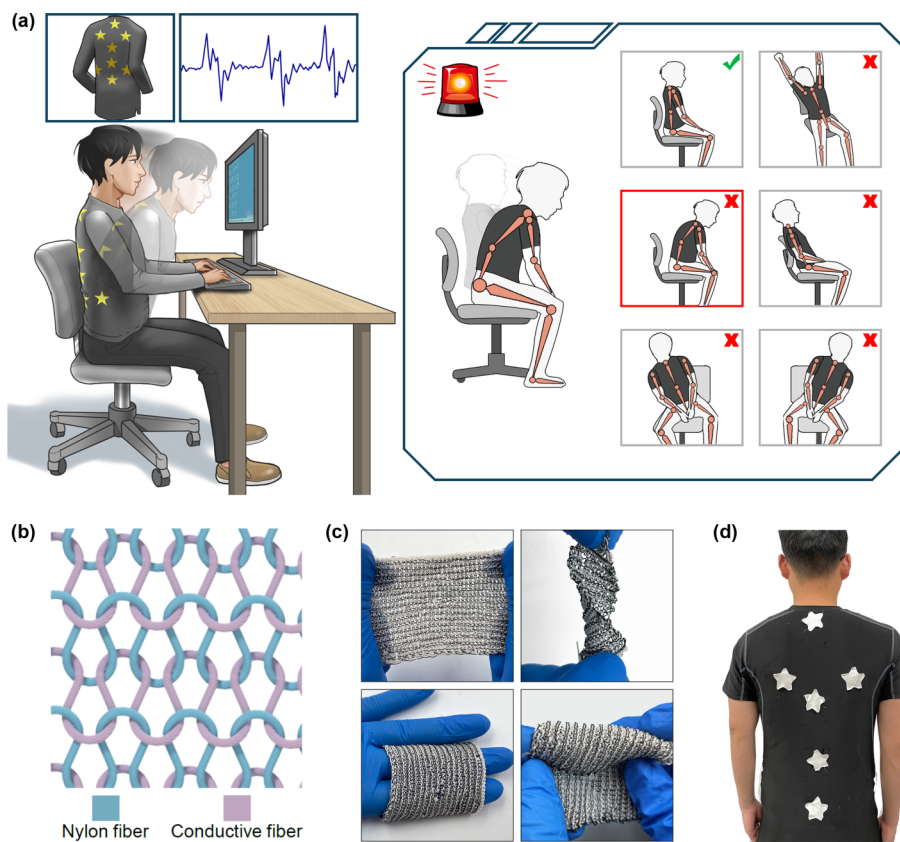


**Figure 1** Fabrication and structure of SPMV. (a) Schematic diagram showing the volunteer wearing the SPMV with various sitting positions. (b) Knitted loop fiber structure with interlaced double threads. (c) Flexibility of fibers during stretching, twisting, rolling, and bending. (d) Different sensor positions of the SPMV.

nylon yarn surface generates induced charges as a result of the potential difference (Fig. 2(d)).

### 3.3 Electrical output and sensing performance

To obtain a quantitative analysis of the electrical output performance of the proposed SPMV, we utilize a linear motor that provides a periodic contact–separation motion. Thereafter, the output of the SPMV is tested at different frequencies to evaluate its output response properties. A distinct difference is observed in the voltage and charge. Additionally, the current of the SPMV increases as the frequency increases from 1–5 Hz (Fig. 2(e)). Figures S1(a)–S1(c) in the Electronic Supplementary Material (ESM) present the detailed data. If the SPMV connects with capacitors or batteries, the generated electricity can be stored. This accumulated and stored charge can be utilized to sustainably power wearable electronics. To study the ability of the SPMV to store charge, its charging curve under different capacitors is plotted. As per the curve, the charging speed decreased as the capacitance increases (Fig. S1(d) in the ESM). Additionally, we evaluate the effective output performance of the SPMV by testing it under different resistances. As the external resistances increase, the current in SI-TENG decreases, whereas the instantaneous power density initially increases and then decreases. The instantaneous power density reaches a maximum of  $2.5 \text{ mW/m}^2$  at a load resistance of  $440 \ \Omega$  (Fig. S1(e) in the ESM). Figure S1(f) in the ESM illustrates the corresponding power circuit.

To evaluate its efficiency and ease of usage, we test various performance parameters of the SPMV, including sensing property, voltage response, washability, stability, and accuracy of response to pressure. Figure 2(f) displays the results of evaluating the sensing property of the SPMV. This figure shows that the voltage increased as the applied pressure increased from 0–80 kPa. This higher voltage output is caused by the formation of larger contact areas due to increased pressure. Furthermore, the response curve

of pressure exhibits two distinct regions. In the low-pressure region (0–20 kPa), the SPMV exhibits a well-behaved linear response with a pressure sensitivity of  $0.16 \text{ mV/Pa}$ ; however, in the high-pressure region ( $> 20 \text{ kPa}$ ), the pressure sensitivity is  $0.05 \text{ mV/Pa}$ . Figure S2 in the ESM presents the output responses of the charge and current under different pressures.

The flexibility, stretchability, and bending ability affect the comfort of wearable sensors. Figure 3(a) displays the results of evaluating the stretchability of SPMV. This figure shows that the SPMV exhibits good stretchability due to its knitting structure, and its output increased with increasing strain. Additionally, it exhibits a favorable response to the curvature and exhibits a higher voltage as the curvature angles increase (Fig. 3(b)). Washability also is important for smart textiles. We evaluate its voltage after washing it in water for 0, 5, and 10 h, respectively. Figure 3(c) displays the washability of the SPMV, which shows that after washing the textile for 10 h, the voltage of the curved textile does not exhibit a noticeable change under different pressures when compared with the unwashed devices.

A stable and accurate response to pressure is vital for smart sensors. Figure 3(d) displays the voltage response of SPMV under different pressures. Further, the voltage response is constant under a fixed pressure and increased with increasing pressure. Figure 3(e) shows an enlarged illustration of the single contact–separation process. Under fixed pressure, the voltage generated by the sensor remained stable, whereas when the applied pressure is zero, the voltage is nearly zero. To clarify the pressure response performance, we further study the relationship between the voltage output and applied pressure. The voltage frequency corresponds to the applied force (Fig. S3 in the ESM). Figure S4 in the ESM displays the corresponding voltage frequency, charge, and current.

As stability and durability are vital parameters for the wearable sensor, we further explore the durability and stability of the SPMV

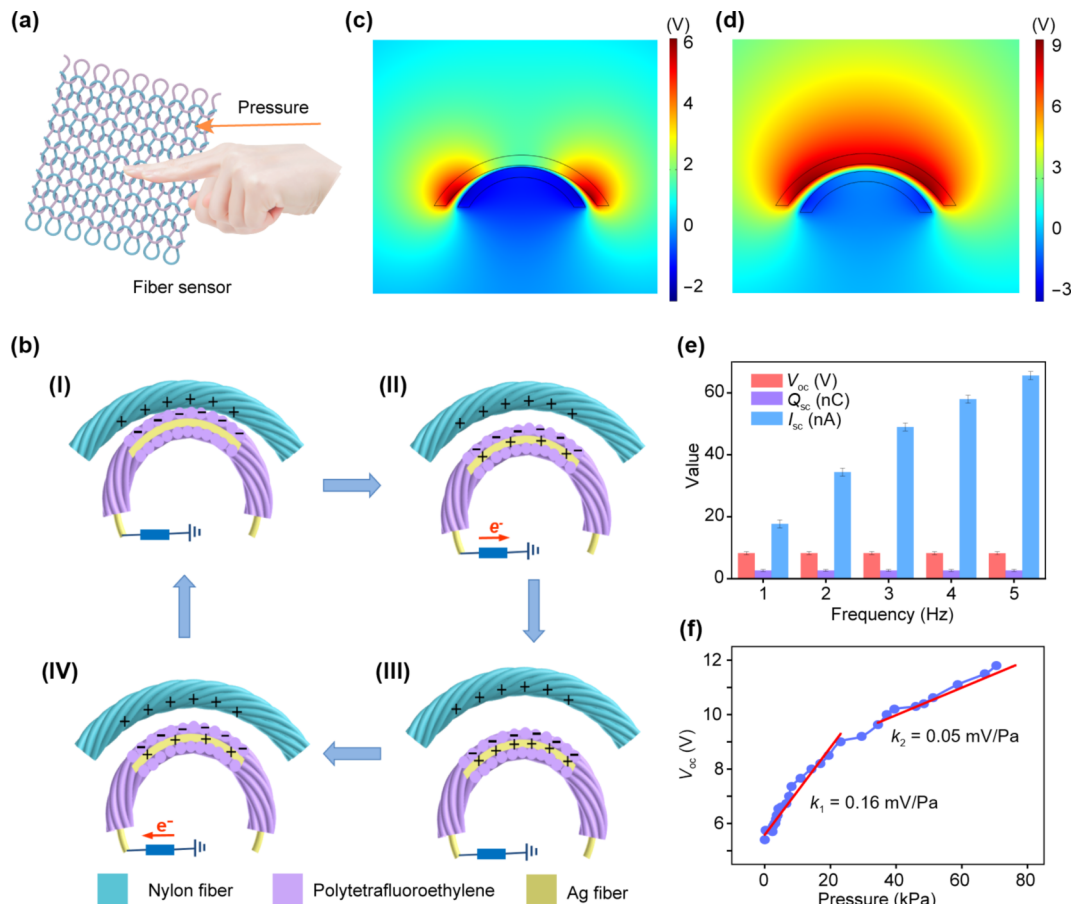


**Figure 2** Demonstrating the working principle of SPMV. (a) Effect of applying pressure on the fiber. (b) Schematic illustrations of transferred charges under different conditions. (c) and (d) Simulation result of the charge distribution of the SPMV under different conditions. (e) Open-circuit voltage ( $V_{oc}$ ), charge transfer ( $Q_{sc}$ ), and short-circuit current ( $I_{sc}$ ) of TENG under the frequency range of 1–5 Hz. (f)  $V_{oc}$  of SPMV under different pressures.

contact–separation cycles under an applied force of 8 N at a frequency of 1 Hz. There is no identifiable change in the current after 12,000 cycles (Fig. 3(f)). Figure 3(g) shows an enlarged illustration of the current. Additionally, the bending cycles remain constant under the frequency of 1 Hz (Fig. 3(h)).

The specifications of the fibers affect the output of the SPMV. We test different sizes of the yarn to prepare the knitted loops to obtain the most suitable fiber specifications for the SPMV. The 150D/2 nylon yarn and the 0.30 mm conductive fiber exhibit the most favorable output under the pressure from 0–80 kPa (Fig. 3(i)). To clarify the effect of knitting density on the output, sensors with different loop numbers are attached in the fabricated area of 2 cm × 2 cm. Figure 3(j) displays the output (voltage, current, and charge) of the sensors with the loop numbers of 50, 100, and 150, respectively. This figure shows that the loop number of 100 exhibits the best output, demonstrating the most suitable density.

Air permeability is a vital parameter for smart textiles. To verify the air permeability, we compare the SPMV with cotton clothing. The SPMV exhibits an air permeability of 580 mm/s under the pressure of 6 Pa, whereas the cotton clothing exhibits an air permeability of 580 mm/s under the pressure of 750 Pa (Fig. 3(k)). This result demonstrates that SPMV has superior air permeability to cotton clothing. What's more, the water vapor transmission of the SPMV is 962 g/(m<sup>2</sup>·h), better than cotton cloth (408 g/(m<sup>2</sup>·h)), shown in Fig. S5 in the ESM.

### 3.4 Analyzing signal of the sitting posture

To analyze the movements of the human body in detail, we position the sensors on different parts of the user's body, including the cervical spine, thoracic spine, and lumbar spine

(Fig. 4(a)). Based on the position of the sensors, the user can monitor posture signals for poor postures, such as humpback, in real time (Fig. 4(b)). Humpback is one of the most common poor sitting postures that can result in spinal deformation and asymmetry. When the user sits in the humpback position or the idle posture, corresponding signals are produced (Fig. 4(c)). The sensors, labeled from 1–8, placed on different parts of the body, exhibit different signals when the user sits forward (Fig. 4(d)). Sensors 1–4 are positioned on the cervical spine (Fig. 4(l)), end part of the thoracic spine (Fig. 4(h)), left shoulder wing (Fig. 4(k)), and right shoulder wing (Fig. 4(g)), respectively. Sensors 5–8 are positioned on the front of the lumbar spine (Fig. 4(j)), left-side waist (Fig. 4(f)), right-side waist (Fig. 4(i)), and end part of the lumbar spine (Fig. 4(e)), respectively. When the wearer sits forward, the textile sensors in the bilateral shoulder wing, cervical spine, and thoracic spine bulge stretch, producing distinct signals (Figs. 4(g), 4(k), 4(l), and 4(h)), respectively. Simultaneously, the sensors positioned on the other parts of the body exhibit a relatively small signal. We analyze the precise changes in the signal sets of the eight-sensor arrays in different sitting postures. Figure S6 in the ESM outlines several poor sitting postures, including user leaning toward the right, user leaning toward the left, and sitting backward, which are studied, along with the ideal posture of stretching and sitting idle.

### 3.5 Real-time monitoring of sitting postures

Figure 5(a) illustrates the process of real-time monitoring of various sitting postures by analyzing the user wearing the proposed SPMV in daily life. When the SPMV generates electronic signals in the eight sensors, the corresponding signal data are processed by the machine learning algorithm. First, the

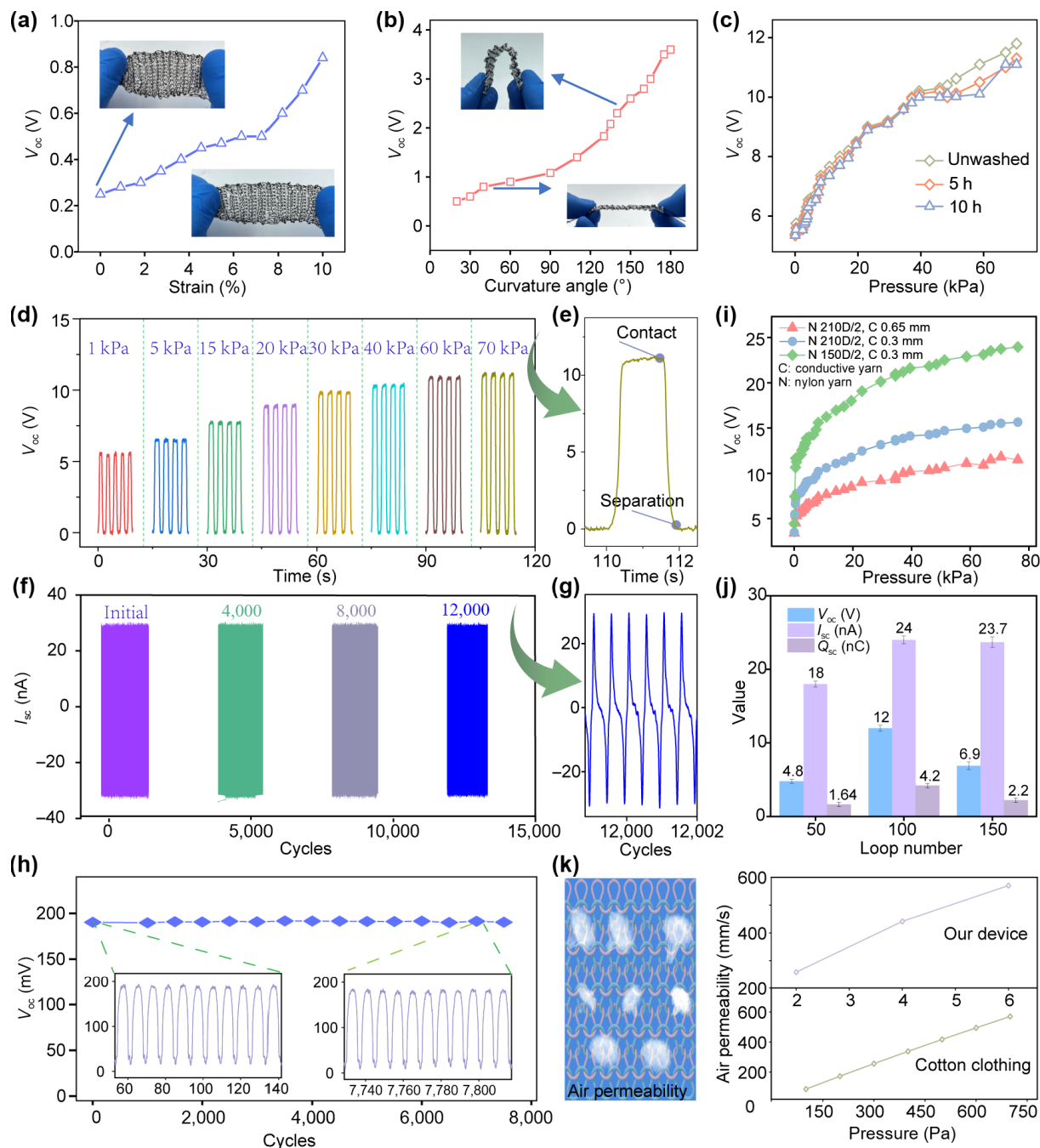


**Figure 3** Electrical and mechanical characterization of SPMV. (a) Output performance of the SPMV under different tensile strains. (b) Output performance of the SPMV under different curvature angles. (c)  $V_{oc}$  of the SPMW under different washing times. (d)  $V_{oc}$  of the SPMW with different applied pressures. (e) Enlarged image of the single cycle of the contact–separation under 70 kPa. (f)  $I_{sc}$  of the SPMV under 12,000 loading cycles. (g) Enlarged image of the loading cycles. (h) The voltage output of the SPMW under 8,000 bending cycles. (i)  $V_{oc}$  under different fibers. (j)  $V_{oc}$ ,  $Q_{sc}$ , and  $I_{sc}$  under various numbers of loop units in the same fabric area. (k) Air permeability of the SPMV and cotton clothing.

data sets are processed using fast Fourier transform and randomly sampled in columns and rows to form multiple training sets, using random forest. Thereafter, these sets are trained using random decision tree to form a random forest that classifies the sitting position through multiple voting decisions of the decision tree, thereby allowing random forest to accurately identify and classify newly obtained data. Finally, we monitor the real-time changes in the sitting posture of the user in response to the screen feedback.

Using the machine learning algorithm, we continuously monitor the sitting posture of the user in real time (Fig. 5(b)). Figure 5(b)(i) displays the records of incorrect posture when the user is leaning toward the right or sitting idle. As per the figure, when the user leans toward the right, the virtual character on the screen leans toward the right as well. Similarly, when the wearer

sits idle, the character mimics their idle position. The enlarged picture of the screen is displayed toward the right of Fig. 5(b)(i). The details of the real-time monitoring and feedback are displayed in Movie EMS1. Figure 5(b)(ii) and Movie EMS2 depict the incorrect posture and corresponding response of the virtual character leaning toward the left. Stretching oneself can stretch the muscles and relax the spine, thereby squeezing the chest organs into the heart and the lung extrusion; this supplies more oxygen to the tissue and organs (Fig. 5(b)(iii) and Movie EMS3). At the same time, due to the movement of the upper limbs and body, more oxygenated blood can be supplied to the brain, thereby resulting in a feeling of awareness and comfort. Figure 5(b)(iv) and Movie EMS4 illustrate the poor sitting posture of a humpback that results in excessive lordosis of the cervical spine and thoracic spine, and

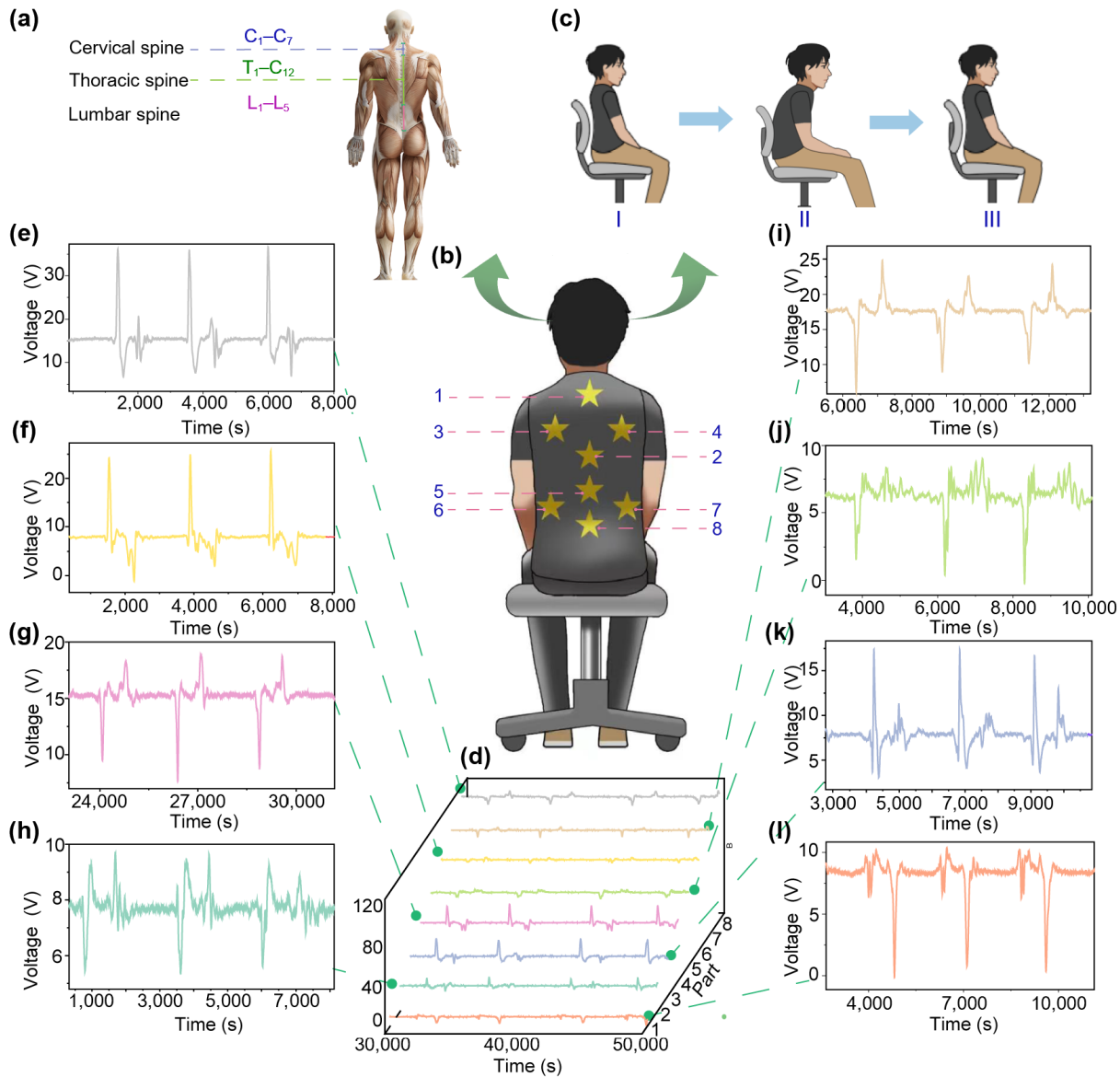


**Figure 4** Analysis of signal response to human sitting posture. (a) Schematic illustration of a human spine model. (b) Humpback posture for the user with the SPMV. (c) Decomposition action of humpback. (d) Eight voltage signals of the different human parts for humpback with sensor arrays. Enlarged images of the corresponding signals: (e) end part of the lumbar spine, (f) left-side waist, (g) right shoulder wing, (h) end part of the thoracic spine, (i) right-side waist, (j) front of the lumbar spine, (k) left shoulder wing, and (l) cervical spine.

causes spine pain and other diseases. Leaning backward is a common incorrect posture as well (Fig. 5(b)(v) and Movie EMS5). Without a cushion to support the lower waist, leaning backward results in inadequate support to the lumbar spine and waist, increasing the pressure on the waist and escalating the risk of the lumbar disc prolapse. When the wearer sits in the idle position, the character mimicked the idle position on the computer (Fig. 5(c) and Movie EMS6). Based on these observations, since maintaining a good posture for longer periods is difficult for individuals, the dynamic virtual character offers an effective method of reminding users to adjust their sitting posture.

Decision tree, which is a basic algorithm for classification and regression, divided the dates into similar subsets to build a complete tree. Random forest, which is an integrated algorithm based on a decision tree classifier, obtained the final result by considering multiple independent decision trees. Due to the inclusive dimensions of characteristic dates, random forest is more suited for processing the signal dates of sitting postures as characteristic dates are not single. Additionally, the trained speed of huge data and their recognition accuracy is comparatively faster in random forest than the other algorithms due to the

synchronous working of the different decision trees. The model trained by random forest achieves a high positive predicted value and a true positive rate for posture recognition (Fig. 5(d)). The recognition accuracy of random forest is 96.6%, which is higher than both the logistic regression (95.5%) and decision tree (94.3%).

## 4 Conclusions

We present a self-powered SPMV based on TENG and machine learning that can accurately recognize and monitor the sitting posture positions of individuals. The SPMV exhibits a high sensitivity of 0.16 mV/Pa, excellent mechanical stretchability, good air permeability, and a bending and twisting characteristic that is favorable for the comfort of wearable devices. Additionally, it produces an accurate electric signal response to different deformations and movements of the user. By positioning the sensors on various parts of clothing, the SPMV collects more information and recognizes precise sitting postures, thereby achieving non-invasive health monitoring and intervention. Combined with the machine learning algorithm, the SPMV

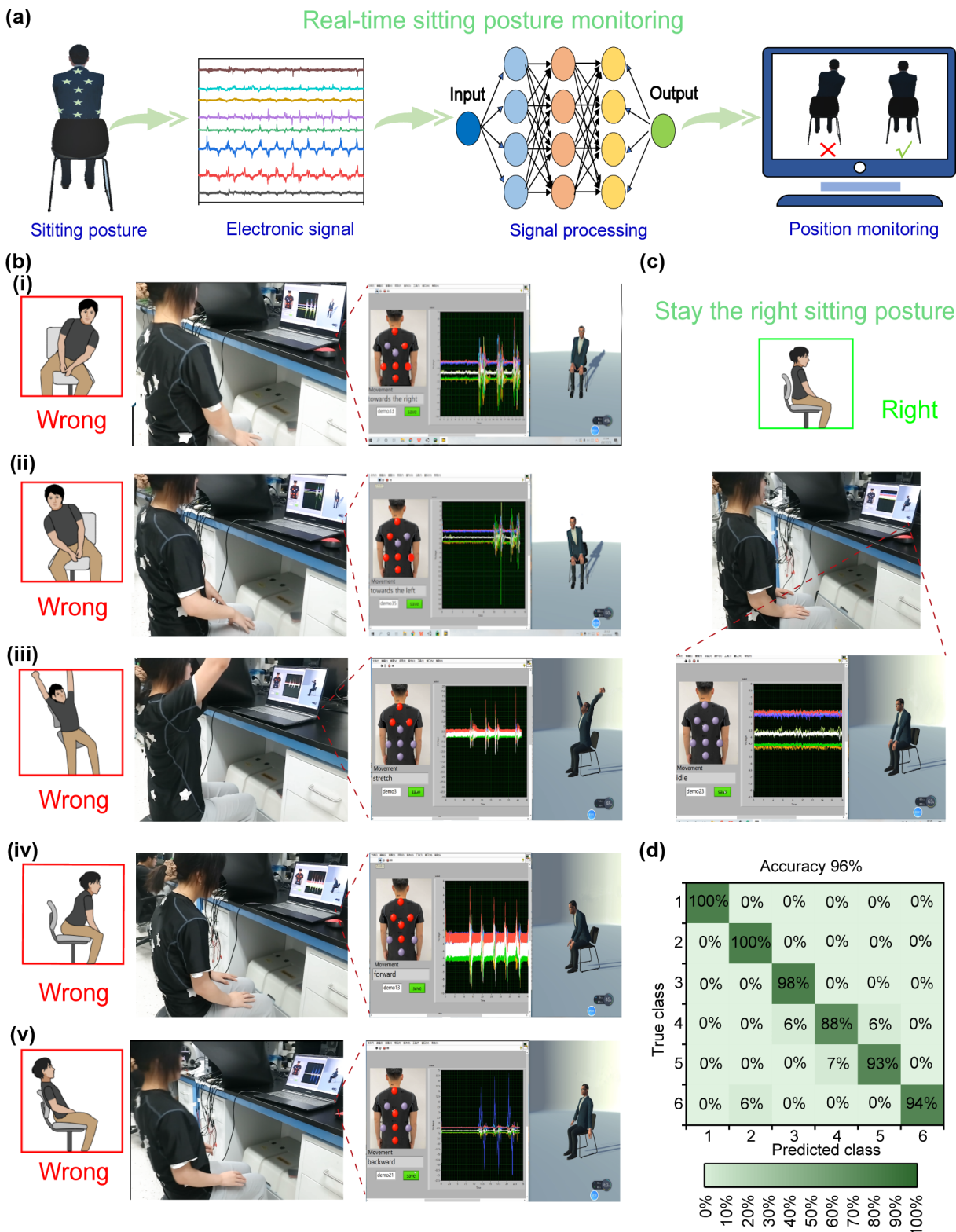


**Figure 5** Real-time monitoring of the sitting posture. (a) Flow chart of the real-time sitting posture monitoring process. (b) Photographs of the virtual character's responses with respect to changes in the user sitting posture at different sitting postures. (c) Correct sitting posture for the user and the virtual character. (d) Confusion map for the machine learning outcomes, the six postures including: (i) toward the right, (ii) toward the left, (iii) humpback, (iv) backward, (iv) sitting idle, and (c) along with the ideal posture of stretching.

monitors various sitting postures in real time. Using the random forest classifier, it achieves a posture recognition accuracy of 96.6%, which is higher than the logistic regression (95.5%) and decision tree (94.3%) classifiers. Thus, we believe that the proposed TENG-based SPMV offers a reliable healthcare solution for long-term non-invasive monitoring, thereby widening the application of triboelectric-based wearable electronics.

### Acknowledgements

The authors are grateful for the support received from the National Key R&D Program of China (No. 2021YFA1201601), the National Natural Science Foundation of China (No. 22109012), Natural Science Foundation of Beijing (No. 2212052), and the Fundamental Research Funds for the Central Universities (No. E1E46805).

**Electronic Supplementary Material:** Supplementary material (output, frequency responses, water vapor transmission, and real-time working demonstration of the SPMW) is available in the online version of this article at <https://doi.org/10.1007/s12274-022-4409-0>.

## References

- [1] Rau, T. R.; Plaschke, K.; Weigand, M. A.; Maier, C.; Schramm, C. Automatic detection of venous air embolism using transesophageal echocardiography in patients undergoing neurological surgery in the semi-sitting position: A pilot study. *J. Clin. Monit. Comput.* **2021**, *35*, 1103–1109.
- [2] Li, F. K.; Sheng, C. S.; Zhang, D. Y.; An, D. W.; Huang, J. F.; Li, Y.; Wang, J. G. Resting heart rate in the supine and sitting positions as predictors of mortality in an elderly Chinese population. *J. Hypertens.* **2019**, *37*, 2024–2031.
- [3] Liutkus, D.; Gouraud, J. P.; Blanloeil, Y.; ANARLF. The sitting position in neurosurgical anaesthesia: A survey of French practice. *Ann. Fr. Anesth. Reanim.* **2003**, *22*, 296–300.
- [4] Wu, C. C.; Chiu, C. C.; Yeh, C. Y. Development of wearable posture monitoring system for dynamic assessment of sitting posture. *Phys. Eng. Sci. Med.* **2020**, *43*, 187–203.
- [5] Roh, J.; Park, H. J.; Lee, K. J.; Hyeong, J.; Kim, S.; Lee, B. Sitting posture monitoring system based on a low-cost load cell using machine learning. *Sensors* **2018**, *18*, 208.
- [6] Kim, Y. M.; Son, Y.; Kim, W.; Jin, B.; Yun, M. H. Classification of children's sitting postures using machine learning algorithms. *Appl. Sci.* **2018**, *8*, 1280.
- [7] Chang, I. S.; Mak, S.; Armanfard, N.; Boger, J.; Grace, S. L.; Arcelus, A.; Chessex, C.; Mihailidis, A. Quantification of resting-state ballistocardiogram difference between clinical and non-clinical populations for ambient monitoring of heart failure. *IEEE J. Transl. Eng. Health Med.* **2020**, *8*, 2700811.
- [8] Zhang, C.; Fan, Y. J.; Li, H. Y.; Li, Y. Y.; Zhang, L.; Cao, S. B.; Kuang, S. Y.; Zhao, Y. B.; Chen, A. H.; Zhu, G. et al. Fully rollable lead-free poly (vinylidene fluoride)-niobate-based nanogenerator with ultra-flexible nano-network electrodes. *ACS Nano* **2018**, *12*, 4803–4811.
- [9] Ning, C.; Dong, K.; Gao, W. C.; Sheng, F. F.; Cheng, R. W.; Jiang, Y.; Yi, J.; Ye, C. Y.; Peng, X.; Wang, Z. L. Dual-mode thermal-regulating and self-powered pressure sensing hybrid smart fibers. *Chem. Eng. J.* **2021**, *420*, 129650.
- [10] Jiang, Y.; Dong, K.; An, J.; Liang, F.; Yi, J.; Peng, X.; Ning, C.; Ye, C. Y.; Wang, Z. L. UV-protective, self-cleaning, and antibacterial nanofiber-based triboelectric nanogenerators for self-powered human motion monitoring. *ACS Appl. Mater. Interfaces* **2021**, *13*, 11205–11214.
- [11] Dong, K.; Hu, Y. F.; Yang, J.; Kim, S. W.; Hu, W. G.; Wang, Z. L. Smart textile triboelectric nanogenerators: Current status and perspectives. *MRS Bull.* **2021**, *46*, 512–521.
- [12] Dong, K.; Peng, X.; Wang, Z. L. Fiber/fabric-based piezoelectric and triboelectric nanogenerators for flexible/stretchable and wearable electronics and artificial intelligence. *Adv. Mater.* **2020**, *32*, 1902549.
- [13] Li, L. L.; Wang, D. P.; Zhang, D.; Ran, W. H.; Yan, Y. X.; Li, Z. X.; Wang, L. L.; Shen, G. Z. Near-infrared light triggered self-powered mechano-optical communication system using wearable photodetector textile. *Adv. Funct. Mater.* **2021**, *31*, 2104782.
- [14] Wang, D. Y.; Wang, L. L.; Shen, G. Z. Nanofiber/nanowires-based flexible and stretchable sensors. *J. Semicond.* **2020**, *41*, 041605.
- [15] Zhou, Z. H.; Chen, K.; Li, X. S.; Zhang, S. L.; Wu, Y. F.; Zhou, Y. H.; Meng, K. Y.; Sun, C. C.; He, Q.; Fan, W. J. et al. Sign-to-speech translation using machine-learning-assisted stretchable sensor arrays. *Nat. Electron.* **2020**, *3*, 571–578.
- [16] Peng, X.; Dong, K.; Ye, C. Y.; Jiang, Y.; Zhai, S. Y.; Cheng, R. W.; Liu, D.; Gao, X. P.; Wang, J.; Wang, Z. L. A breathable, biodegradable, antibacterial, and self-powered electronic skin based on all-nanofiber triboelectric nanogenerators. *Sci. Adv.* **2020**, *6*, eaba9624.
- [17] Jiang, Q.; Yuan, H. L.; Dong, K.; Lin, J. H.; Wu, L. W.; Tang, Y. H. Continuous and scalable manufacture of aggregation induced emission luminogen fibers for anti-counterfeiting and hazardous gas detecting smart textiles. *Mater. Des.* **2021**, *205*, 109761.
- [18] Jang, K. I.; Li, K.; Chung, H. U.; Xu, S.; Jung, H. N.; Yang, Y. Y.; Kwak, J. W.; Jung, H. H.; Song, J.; Yang, C. et al. Self-assembled three dimensional network designs for soft electronics. *Nat. Commun.* **2017**, *8*, 15894.
- [19] Hong, S. Y.; Lee, Y. H.; Park, H.; Jin, S. W.; Jeong, Y. R.; Yun, J.; You, I.; Zi, G.; Ha, J. S. Stretchable active matrix temperature sensor array of polyaniline nanofibers for electronic skin. *Adv. Mater.* **2016**, *28*, 930–935.
- [20] Wang, S. H.; Xu, J.; Wang, W. C.; Wang, G. J. N.; Rastak, R.; Molina-Lopez, F.; Chung, J. W.; Niu, S. M.; Feig, V. R.; Lopez, J. et al. Skin electronics from scalable fabrication of an intrinsically stretchable transistor array. *Nature* **2018**, *555*, 83–88.
- [21] Roh, E.; Hwang, B. U.; Kim, D.; Kim, B. Y.; Lee, N. E. Stretchable, transparent, ultrasensitive, and patchable strain sensor for human-machine interfaces comprising a nanohybrid of carbon nanotubes and conductive elastomers. *ACS Nano* **2015**, *9*, 6252–6261.
- [22] Miyamoto, A.; Lee, S.; Cooray, N. F.; Lee, S.; Mori, M.; Matsuhisa, N.; Jin, H.; Yoda, L.; Yokota, T.; Itoh, A. et al. Inflammation-free, gas-permeable, lightweight, stretchable on-skin electronics with nanomeshes. *Nat. Nanotechnol.* **2017**, *12*, 907–913.
- [23] Liu, Y.; Hu, Y.; Zhao, J. J.; Wu, G.; Tao, X. M.; Chen, W. Self-powered piezoionic strain sensor toward the monitoring of human activities. *Small* **2016**, *12*, 5074–5080.
- [24] Ahmad, J.; Andersson, H.; Sidén, J. Screen-printed piezoresistive sensors for monitoring pressure distribution in wheelchair. *IEEE Sens. J.* **2019**, *19*, 2055–2063.
- [25] Salvatore, G. A.; Münzenrieder, N.; Kinkeldei, T.; Petti, L.; Zysset, C.; Strebel, I.; Büthe, L.; Tröster, G. Wafer-scale design of lightweight and transparent electronics that wraps around hairs. *Nat. Commun.* **2014**, *5*, 2982.
- [26] Takei, K.; Takahashi, T.; Ho, J. C.; Ko, H.; Gillies, A. G.; Leu, P. W.; Fearing, R. S.; Javey, A. Nanowire active-matrix circuitry for low-voltage macroscale artificial skin. *Nat. Mater.* **2010**, *9*, 821–826.
- [27] Gu, L. L.; Tavakoli, M. M.; Zhang, D. Q.; Zhang, Q. P.; Waleed, A.; Xiao, Y. Q.; Tsui, K. H.; Lin, Y. J.; Liao, L.; Wang, J. N. et al. D arrays of 1024-pixel image sensors based on lead halide perovskite nanowires. *Adv. Mater.* **2016**, *28*, 9713–9721.
- [28] Yang, Z. W.; Pang, Y. K.; Zhang, L. M.; Lu, C. X.; Chen, J.; Zhou, T.; Zhang, C.; Wang, Z. L. Tribotronic transistor array as an active tactile sensing system. *ACS Nano* **2016**, *10*, 10912–10920.
- [29] Pang, C.; Koo, J. H.; Nguyen, A.; Caves, J. M.; Kim, M. G.; Chortos, A.; Kim, K.; Wang, P. J.; Tok, J. B. H.; Bao, Z. N. Highly skin-conformal microhairy sensor for pulse signal amplification. *Adv. Mater.* **2015**, *27*, 634–640.
- [30] Lai, Y. C.; Deng, J. N.; Zhang, S. L.; Niu, S. M.; Guo, H. Y.; Wang, Z. L. Single-thread-based wearable and highly stretchable triboelectric nanogenerators and their applications in cloth-based self-powered human-interactive and biomedical sensing. *Adv. Funct. Mater.* **2017**, *27*, 1604462.
- [31] Jeong, J. W.; Kim, M. K.; Cheng, H. Y.; Yeo, W. H.; Huang, X.; Liu, Y.; Zhang, Y.; Huang, Y.; Rogers, J. A. Capacitive epidermal electronics for electrically safe, long-term electrophysiological measurements. *Adv. Healthc. Mater.* **2014**, *3*, 642–658.
- [32] Wang, Z. L. On Maxwell's displacement current for energy and sensors: The origin of nanogenerators. *Mater. Today* **2017**, *20*, 74–82.
- [33] Zou, H. Y.; Zhang, Y.; Guo, L. T.; Wang, P. H.; He, X.; Dai, G. Z.; Zheng, H. W.; Chen, C. Y.; Wang, A. C.; Xu, C. et al. Quantifying the triboelectric series. *Nat. Commun.* **2019**, *10*, 1427.
- [34] Wang, Z. L. From contact electrification to triboelectric nanogenerators. *Rep. Prog. Phys.* **2021**, *84*, 096502.
- [35] Wang, Z. L. On the first principle theory of nanogenerators from Maxwell's equations. *Nano Energy* **2020**, *68*, 104272.
- [36] Luo, J. J.; Wang, Z. L. Recent advances in triboelectric nanogenerator based self-charging power systems. *Energy Storage Mater.* **2019**, *23*, 617–628.

- [37] Dong, K.; Deng, J. N.; Zi, Y. L.; Wang, Y. C.; Xu, C.; Zou, H. Y.; Ding, W. B.; Dai, Y. J.; Gu, B. H.; Sun, B. Z. et al. 3D orthogonal woven triboelectric nanogenerator for effective biomechanical energy harvesting and as self-powered active motion sensors. *Adv. Mater* **2017**, *29*, 1702468.
- [38] Cong, Z. F.; Guo, W. B.; Guo, Z. H.; Chen, Y. H.; Liu, M. M.; Hou, T. T.; Pu, X.; Hu, W. G.; Wang, Z. L. Stretchable coplanar self-charging power textile with resist-dyeing triboelectric nanogenerators and microsupercapacitors. *ACS Nano* **2020**, *14*, 5590–5599.
- [39] Gunawardhana, K. R. S. D.; Wanasekara, N. D.; Dharmasena, R. D. I. G. Towards truly wearable systems: Optimizing and scaling up wearable triboelectric nanogenerators. *iScience* **2020**, *23*, 101360.
- [40] Li, C. Y.; Liu, D.; Xu, C. Q.; Wang, Z. M.; Shu, S.; Sun, Z. R.; Tang, W.; Wang, Z. L. Sensing of joint and spinal bending or stretching via a retractable and wearable badge reel. *Nat. Commun.* **2021**, *12*, 2950.
- [41] Petropoulos, A.; Sikeridis, D.; Antonakopoulos, T. Wearable smart health advisors: An IMU-enabled posture monitor. *IEEE Consum. Electron. Mag.* **2020**, *9*, 20–27.
- [42] Kim, W.; Jin, B.; Choo, S.; Nam, C. S.; Yun, M. H. Designing of smart chair for monitoring of sitting posture using convolutional neural networks. *Data Technol. Appl.* **2019**, *53*, 142–155.
- [43] Jung, Y. H.; Hong, S. K.; Wang, H. S.; Han, J. H.; Pham, T. X.; Park, H.; Kim, J.; Kang, S.; Yoo, C. D.; Lee, K. J. Flexible piezoelectric acoustic sensors and machine learning for speech processing. *Adv. Mater.* **2020**, *32*, 1904020.
- [44] Ran, X.; Wang, C.; Xiao, Y.; Gao, X. L.; Zhu, Z. Y.; Chen, B. A portable sitting posture monitoring system based on a pressure sensor array and machine learning. *Sens. Actuators A* **2021**, *331*, 112900.
- [45] Loke, G.; Khudiyev, T.; Wang, B.; Fu, S.; Payra, S.; Shaoul, Y.; Fung, J.; Chatziveroglou, I.; Chou, P. W.; Chinn, I. et al. Digital electronics in fibres enable fabric-based machine-learning inference. *Nat. Commun.* **2021**, *12*, 3317.